Journal of Catalysis **201,** 183–197 (2001)
doi:10.1006/jcat.2001.3243, available online at http://www.idealibrary.com on IDEAL®

Decomposition of Methane over Iron Catalysts at the Range of Moderate Temperatures: The Influence of Structure of the Catalytic Systems and the Reaction Conditions on the Yield of Carbon and Morphology of Carbon Filaments

Marina A. Ermakova,[1] Dmitry Yu. Ermakov, Andrey L. Chuvilin, and Gennady G. Kuvshinov

Boreskov Institute of Catalysis, Prosp. Ak. Lavrentieva, 5, 630090 Novosibirsk, Russia

Received August 2, 2000; revised March 1, 2001; accepted April 12, 2001

Decomposition of high-purity methane in the presence of α-Fe-based catalysts to produce filamentous carbon was investigated. The reaction was studied in the temperature range of 650 to 800°C. Filamentous carbon was demonstrated to form at temperatures not lower than 680°C in the presence of both bare α-Fe and catalysts based thereon with admixtures of various hard-to-reduce oxides (SiO_2, Al_2O_3, ZrO_2, andTiO_2). The maximal carbon yield, 45 g per g of iron, was obtained with the Fe/SiO_2 catalyst comprising silica in amounts of 15 wt%. XRD and high-resolution electron microscopy were used for studying the carbon deposits. The data obtained allowed the conclusion on the essential influence of the chemical nature of the hard-to-reduce oxide admixture in the iron catalyst on the microstructure and morphology of the carbon filaments. Depending on the admixture, specific shapes of filaments and nanotubes predominated. Carbon nanotubes with thin walls built up by coaxial cylindrical graphene layers were formed in large amount over the Fe/Al_2O_3 catalyst. Centers of growth of *octopus*-like nanotubes were observed.

Key Words: **methane decomposition; filamentous carbon; iron catalysts; carbon yield; carbon nanotubes; octopus carbon.**

1. INTRODUCTION

The history of catalytic filamentous carbon may be traced back to 1889 when the method for synthesis of filamentous carbon by pyrolysis of a mixture of methane and hydrogen in an iron crucible was patented (1). Since that time, metals of the iron group and the alloys were often used as catasysts for the decomposition of hydrocarbons and carbon monoxide (2) to produce filamentous carbon. The advent of electron microscopy made it possible to discover and describe a number of morphological types of carbon filaments. It became clear that carbon filaments grow as follows: Carbon atoms generated by dissociative chemisorption of hydrocarbons on particular edges of the metal particle diffuse to the opposite planes and crystallize there as continuous graphite-like structures. The mechanism is as yet a disputable point because the nature of the driving force of this process is not well understood.

Methane, which is the most stable hydrocarbon, is the main component of natural gas. The large amounts available make the catalytic decomposition of methane to form hydrogen and filamentous carbon of the most practical interest. A number of recent studies in the field are known. It should be emphasized that conventional catalysts used for methane decomposition are nickel or nickel–copper systems since nickel, among the other metals, is the most active and provides the highest carbon yield (3–9). As to iron-catalyzed decomposition of methane, it was usually achieved at high temperatures (above 1000°C) using methane mixed with hydrogen. Gadelle (10) summarized some results obtained in this field. He believed that the fast growth of carbon filaments started at the point when the iron particle was transformed into the liquid state after having been saturated by carbon. Gadelle's calculations showed that the finest iron particles (6 nm) are fluidized at 1020°C. From the data of Benissad (11) and Tibbets (12), the decomposition of methane on iron particles (6–25 nm) gave rise to the growth of filamentous carbon at the temperature range between 1020 and 1100°C. Lately, Tibbets observed (13) that coarser iron particles (60–100 nm) were also capable of catalyzing the formation of filamentous carbon from the methane–hydrogen mixture. The carbon yield increased sharply at 1140°C to reach its maximum at the point of 1150°C corresponding to the eutectic of the Fe–C alloy. When the temperature was 30° lower, the carbon growth was practically stopped. Earlier, Tibbets *et al.* (12) assumed that the active phase, catalyzing decomposition of hydrocarbons at above 912°C, was γ-Fe (austenite) supersaturated with carbon. However, below this temperature, there was the second maximum of the catalytic activity to formation of filaments, the active phase in this case was α-Fe supersaturated with carbon. Some researchers reported the

[1] To whom correspondence should be addressed. E-mail: erm@catalysis.nsk.su.

0021-9517/01 $35.00

maximal activity in the temperature range of 600 to 700°C for decomposition of CO and hydrocarbons on iron (14–16). The iron activity was extremely low below this range, and the catalysts were rapidly deactivated above it. Several reasons for the deactivation can be enumerated: the sintering of catalyst particles, the formation of pyrolytic carbon black from all the hydrocarbons, except methane, which poisons the catalyst, and, probably, the formation of more stable iron carbide. Unfortunately, there are few data available in the literature on methane decomposition below 900°C. Very contradictory conclusions were made by different researchers. For example, Robertson *et al*. (17) and Evans *et al*. (18) supposed that impurities in methane bear exceptional responsibility for the growth of filaments on nickel and iron below 900°C. However, one could hardly imagine that an impurity in the amount of 0.01% might be responsible for the quantitative decomposition of methane (7). Baker and Thomas (19), who studied the decomposition of methane over iron particles supported on silicon at 600 to 1277°C and 40 to 760 torr, said that flocculent amorphous carbon was observed near the iron particles at low temperatures and atmospheric pressure; filaments grew at high temperatures and low pressure. Galuszka and Back (20) reported the growth of carbon filaments from methane at 830°C on iron films pretreated using various kinds of redox procedures. Sacco *et al*. (21), while studying the growth of filamentous carbon through the decomposition of multicomponent gas mixtures containing methane in different proportion on iron foil at 627°C, concluded that methane, if without considerable addition of CO, did not produce filaments. Recently, Avdeeva and Shaikhutdinov (22) synthesized hollow filaments over 50% Fe/Al_2O_3 catalyst at 600°C, methane being quantitatively decomposed to form carbon. The yield of carbon reached 10 g per g of metal in this case. The authors gave no detail on the catalyst composition.

The natural conclusion made on the basis of the data available is that bulky iron as itself cannot catalyze the decomposition of methane to form carbon filaments. To initiate this process, one must make iron dispersed. The addition of carbon monoxide to methane or the oxidation of bulky iron followed by reduction can be used for this purpose. On the other hand, Hernadi *et al*. (23) observed decomposition of acetylene, propylene, and ethylene but not methane over a highly dispersed 2.5% Fe/SiO_2 catalyst at 700°C.

Thus, various researchers come to very contradictory conclusions, even those regarding the possibility of methane decomposition over iron at temperatures below 1000°C. Systematic data which would be helpful for elucidation of this problem, as well as information concerning the catalysts for this reaction, are practically unavailable in the literature. It is quite unclear how the catalyst structure influences, if it does so, the process of filament growth and the carbon morphology. For the above-mentioned studies, iron foils and films, as well as particles supported on various substrates were mainly used as catalysts. Heterogeneous catalysts are, typically, systems comprising an active component and a refractory oxide at a certain proportion. Therefore, it is important to know how the chemical nature of the textural promoter, as well as its proportion in the catalyst, affects the catalytic process. Our previous study (7) in the field of methane decomposition allows a distinct relationship between the structure of nickel catalysts and the yield of filamentous carbon to be elucidated. We showed that the longest catalyst lifetime during methane decomposition was attained using Ni/SiO_2 systems with high (90%) nickel loading and the optimal particle size (30–60 nm) in the starting catalyst. The carbon yield reached 380 g per g of nickel over these catalysts. It was reasonable to suppose that similar regularities were valid for the iron-based catalysts.

The present work is aimed at studying the influence of the structure and composition of iron catalysts on the yield and morphology of filamentous carbon produced by decomposition of methane at moderate temperatures.

2. EXPERIMENTAL

2.1. Catalyst Preparation

Iron hydroxides prepared by precipitation of $FeCl_3 \cdot 6H_2O$ or $Fe(NO_3)_3 \cdot 6H_2O$ with an aqueous ammonia solution were used for synthesis of iron catalysts. In addition, NaOH and KOH were used for precipitation $FeCl_3 \cdot 6H_2O$. The precipitates were carefully washed with water then, in some cases, with an organic solvent, dried, and calcined in a muffle at 300°C for 4 h.

The texture of iron oxide prepared in this way (hematite $Fe_2O_3 \cdot nH_2O$) was varied by calcining it in air for an hour at different temperatures ranging from 300°C to the melting point to form magnetite (Fe_3O_4).

Catalysts were prepared by the heterophase sol–gel method (24) based on impregnation of a porous precursor of the active component, iron oxide in this case, with the precursor of a textural promoter taken in the estimated amount. The role of the textural promoter was to stabilize the active component structure and to prevent its sintering in the course of posttreatments. Hard-to-reduce oxides (HRO) such as silica, alumina, titanium dioxide, and zirconium oxide were used as textural promoters. Impregnation was conducted using an alcohol solution of prehydrolized tetraethoxysilane (TEOS) as a supplier of silica, solution of aluminium isopropylate in hexane as a supplier of alumina, solution of titanium ethoxide in xylene as a supplier of titanium dioxide, aqueous solution of zirconyl nitrate as a supplier of zirconium oxide. The next steps were drying of the precursors at room temperature and reduction

in hydrogen at various temperatures ranging from 700 to 1100°C.

2.2. Catalysts Testing

Catalysts were tested in a fluidized bed at 600–800°C using a laboratory installation with a flow quartz reactor. The working zone of the reactor was 20 cm^3. Catalysts in the oxide or reduced state were loaded in amounts of 0.015 g on the basis of pure iron. High-purity methane (99.99%) was used for decomposition. Methane consumption was preset at 12 cm^3/min in all the cases. The concentration of hydrogen in the mixture was determined using a chromatographic column filled with Na*X* zeolite. The reaction was stopped as soon as the outlet concentration of hydrogen reached 2%. The amount of carbon deposited on the catalyst during the reaction time was determined by weighing unloaded samples.

2.3. Characterization of Catalysts and Carbon

Textural parameters of samples were studied by low-temperature adsorption of nitrogen at 77 K using an automated installation ASAP-2400.

Phase composition of samples and morphology of carbon filaments were studied using XRD with CuK_α radiation ($\lambda = 0.15418$ nm), a graphite crystal monochromator, and silicon as an internal reference. Average size of iron and iron oxide particles was calculated by the Sherrer equation based on semiwidths of diffraction peaks (104), (110) for α-Fe_2O_3 and (110) for α-Fe. The interplane distance (d_{002}) between graphene layers of carbon filaments was determined from the diffraction peak (002) by the Bragg equation.

Thermogravimetric studies of catalyst reduction were carried out using a thermoanalytic system Netzsch STA-409 in the pure hydrogen atmosphere in the temperature programmed mode at the rate of temperature elevation equal to 5°C/min.

Micrographs were recorded using transmission electron microscopes JEM-100CX and JEM-2010.

3. RESULTS AND DISCUSSION

3.1. Influence of Conditions of Preparation of the Active Component Precursor, Its Texture and Reaction Temperature on the Yield of Carbon

As was described above, an aqueous ammonia solution, as well as potassium and sodium hydroxides, was used for precipitating iron hydroxide. The precipitate was immediately washed with distilled water on a Nutsch filter. Precipitates obtained with the alkali metal hydroxides were washed more carefully to remove the alkali ions. However, the alkali metal ions could not be removed completely due to their strong chemisorption on the surface of amorphous goethite particles. It should be pointed out that the washing and dilution of the electrolyte is accompanied by the formation of a sol which blocks up the pores and makes it hardly possible to wash the precipitate. That was why the concentrations of Na and K ions remained large enough, 1 and 0.7%, respectively, even though the washing stage was long. Table 1 demonstrates a very unfavorable effect of these ions on the ability of these iron catalysts to decompose methane for the production of filamentous carbon. A higher deactivating effect is seen to be characteristic of potassium compared to that of sodium. Notice that the introduction of alkali metal impurities into catalysts for oxidative conversion of methane and into Fisher-Tropsch catalysts also results in a suppression of coke formation. Therefore, the catalysts prepared by precipitation of iron hydroxide with ammonia were only used for the further studies of the formation of filamentous carbon. The iron salts were Fe(III) chloride or nitrate. Table 1 shows that the nature of the salt does not influence the carbon yield on the reduced catalyst.

Figure 1 is a thermogram of reduction of iron oxide (hematite Fe_2O_3) precalcined in air at 450°C for 1 h. Two main maxima in the rate of sample weight loss, the first at 292.5°C and the second at 495.4°C, are seen in the DTG curve. A total of the weight loss is ca. 36% that corresponds to the composition of the initial sample $Fe_2O_3 \times H_2O$. The

TABLE 1

Influence of Conditions of Iron Oxide Preparation on the Yield of Carbon at 700°C

Iron salt	Precipitator	Calcination temperature in °C	Specific surface area in m^2/g	Average size of Fe_2O_3 particles, nm	Carbon yield, gC/gFe
$FeCl_3 \cdot 6H_2O$	NaOH	300	37	46 (hematite)	1
$FeCl_3 \cdot 6H_2O$	KOH	300	40	43 (hematite)	0.25
$FeCl_3 \cdot 6H_2O$	NH_4OH	300	106	X-ray amorphous	16.5
$FeCl_3 \cdot 6H_2O$	NH_4OH	450	61	29 (hematite)	16.8
$FeCl_3 \cdot 6H_2O$	NH_4OH	700	8.6	98 (hematite)	16.6
$FeCl_3 \cdot 6H_2O$	NH_4OH	900	0.7	>100 (hematite)	16.5
$FeCl_3 \cdot 6H_2O$	NH_4OH	1600	<0.1	>100 (magnetitite)	16.7
$Fe(NO_3)_3 \cdot 6H_2O$	NH_4OH	450	65	27 (hematite)	17

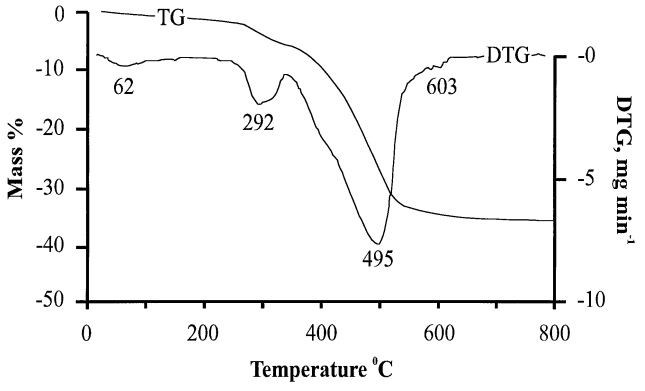

FIG. 1. Thermogravimetric curves of reduction of Fe_2O_3 by hydrogen. The oxide sample was precalcined at 450°C.

first reduction stage finishes at ca. 360°C; the sample loses ca. 6% of its weight that corresponds to a partial elimination of water during the $Fe_2O_3 \rightarrow Fe_3O_4$ transition. The major sample weight loss is observed at the second stage during the transition to α-Fe. Thus, it is obvious that iron is fully reduced by the starting point of the reaction.

A number of experiments were carried out at different temperatures in the range of 650 to 800°C in order to determine the optimal reaction temperature providing the maximal carbon yield. The carbon yield is still low at 670°C (Fig. 2). In this case the catalyst activity is low and it is fully deactivated in 3 h. As little as 10°C temperature elevation results in many times increase in the carbon yield, which reaches a maximum. This is a striking feature of the process under study. The opposite case is methane decomposition on nickel catalysts when temperature-lowering results in a decrease in the activity while the carbon yield remains the same (8). This fact indicates different mechanisms of growth of filamentous carbon on nickel and iron particles.

Elevation of the reaction temperature up to 800°C leads gradually to a decrease in the filament yield. Unfortunately, the further temperature elevation was not allowed with the available facilities. Thus, the temperature range from 680 to 700°C may be considered as optimal for the process of methane decomposition on α-Fe.

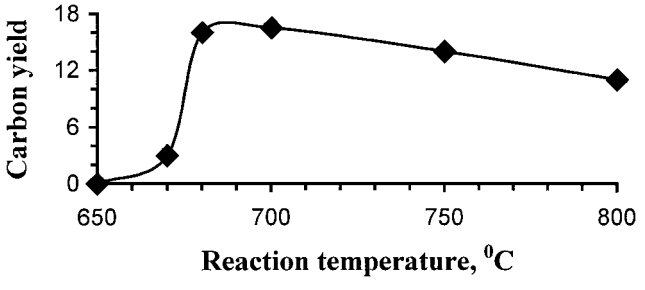

FIG. 2. Yield of carbon (g/g Fe) on the textural promoter-free catalyst as a function of reaction temperature.

Another problem under study was to elucidate if it is possible to influence the yield of carbon by varying the texture of the active component precursor (iron oxide). It is seen in Table 1 that the texture of iron oxide was varied over a wide range while the yield of carbon remains approximately the same for all the samples. All the catalysts behaved in the same manner. At the early stage of the reaction, the catalyst activity increased to reach a stable maximum at ca. 0.3 mol $CH_4/h \cdot g$ Fe in 6 or 7 h. Hence, the size of the formed iron particles seems to be independent of the precursor texture and determined only by the reduction temperature. In the present case, the oxide samples were reduced at the temperature equal to the temperature of methane decomposition, i.e., to 700°C. When the reduction temperature was elevated to 800°C, the catalyst reached its maximal activity during a longer period of time (9 h) but then it behaved in the same manner as the other catalysts. If the reduction temperature was elevated to 1100°C, the catalyst activity was low even at the reaction temperature of 750°C and did not increase during a long period of time; hence, iron remained partly in the inactive state. Probably, the liability of iron particles to carbidization under the action of methane decreases as they grow in size. Since the presence of the metastable carbide phase on iron is a necessary condition of the growth of filamentous carbon, the carbon yield falls down to reach zero at a decrease in the carbide content in the catalyst.

3.2. Influence of Promoting Admixtures of Hard-to-Reduce Oxides on the Yield of Carbon

Special experiments were carried out to understand how the introduction of textural promoters influences the behavior of iron catalysts during decomposition of methane. Various hard-to-reduce oxides chosen among compounds widely used for preparing catalyst supports were introduced into samples of iron oxides with certain textures preformed by the heterophase sol–gel method. Notice that fresh iron hydroxide precipitate consists of the finest structural units, which are 2–3 nm in size (25). If there was water in the pores of the precipitate, the huge compression during drying made the precipitate dense, glassy, and possessing a high specific surface area (400–500 m^2/g) built-up predominantly by fine pores. After calcinations at 300°C, the surface area decreased to 70 m^2/g and the pore volume was 0.3 ml/g. Such a pore volume restricted considerably the potential introduction of the required amount of textural promoters into the oxide. To prevent the shrinkage, water was displaced from the pores by successive washing of the precipitate with polar and nonpolar organic solvents. As a result, pore volume of up to 3.5 ml/g and surface area of 106 m^2/g were characteristic of the iron oxide calcined at 300°C. Such a pore volume allowed the metal to textural promoter ratio to be varied over a wide range in the reduced catalyst. That was the

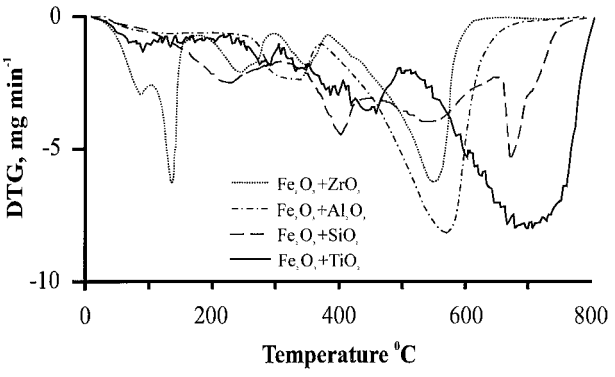

FIG. 3. Thermogravimetric curves of reduction of promoted iron catalysts with hydrogen.

starting point of our studies. A number of iron oxide samples with textural parameters varied over wide ranges were prepared by varying the calcination temperature (Table 1).

Iron–silica systems were carefully studied in order to understand the influence of textural promoters on the yield of carbon. The reason for choosing silica was that it appeared the most appropriate textural promoter for similar nickel-based catalysts (7).

A DTG curve (Fig. 3) demonstrates the reduction of an iron-oxide sample containing SiO_2 in amount of 15% on the basis of pure iron. Four main peaks of the rate of weight loss are seen in the curve at 231, 404, 560, and 676°C. Thus, the catalyst undergoes a series of successive transformations including $Fe_2O_3 \rightarrow Fe_3O_4$ at 3.49% (calculated 3.3%) weight loss, $Fe_3O_4 \rightarrow FeO$ at 6.46% (calculated 6.9%) weight loss, and $FeO \rightarrow \alpha$-Fe. The last stage is thought to include two steps: (1) reduction of silica-unbound Fe and (2) reduction of silicate species. Total weight loss is 18.35% at this stage, while the theoretical value equals 22.3%. Such a discrepancy indicates that, probably, a minor portion of iron remains in the unreduced state. Unfortunately, the use of high reduction temperature lowers the possibility of varying the average particle size in the reduced catalysts, and the size range is shifted to large values. Silica cannot effectively prevent sintering of metal particles at this temperature. For example, the minimal average size of iron particles, 40–50 nm, was attained at 15% content of SiO_2 in the catalyst, while the particles of iron oxide (the catalyst precursor), calculated from the surface area of 106 m^2/g, was 12–15 nm in size. Figure 4 shows the yield of carbon as a function of specific surface area of iron oxide, which was then stabilized with SiO_2 introduced in the proportion of 10 wt% of SiO_2 per 90 wt% of Fe. Silica was introduced into pores of iron oxide samples (see the textural parameters of samples 3–8 in Table 1). A smooth maximum of the carbon yield is seen in the range of 20 to 60 m^2/g that corresponds to the calcinations temperature of 450–600°C, respectively. The carbon yield reaches 30 g/g Fe, i.e., it is two times higher than the yield on bare iron (16–17 g C/g Fe). Even though the carbon yield correlates evidently with textural parameters of silica-stabilized iron oxide, we failed to establish such a correlation for the same catalysts in their reduced state. XRD data demonstrate almost equal average size of iron particles (40–50 nm) in the reduced catalysts. One can explain this discrepancy if one assumes that there is a complex relationship between the yield of carbon and the proportion of silicate species in the catalyst. Apparently, iron–silica catalysts are not completely reduced even at high temperatures, and silicate species are always present in some proportion in the catalysts. The presence of these species may affect the process of filamentous carbon growth. It is logical that the interaction between the active component and silica is stronger when the high-dispersed precursor, but not coarse iron oxide with a low surface area, was used. The corresponding reduced catalysts contain silicate species in different amounts and, therefore, the silicate species influence the formation of carbon filaments in different manners.

Darken (26) discovered as long ago as 1949 that silicon in the form of silicates comprised in iron particles exerts great influence on the thermodynamic activity of carbon dissolved in iron. Baker *et al.* (27) assumed a decrease in the carbon solubility and lowering of the rate of carbon diffusion through the catalytic particle to be a result of the interaction between the support and Fe_2SiO_4 formed by the reaction of α-Fe with silica at 600°C. Baker *et al.* (27) assumed, that Fe_2SiO_4 formed by the interaction of α-Fe with silica support decreased the carbon solubility and lowered the rate of carbon diffusion through the catalytic particle. Kepinski (28) concluded that silica could impede the formation of surface carbide and, eventually, suppressed the growth of carbon filaments. We assume that the influence of nonreduced compounds on the formation of filamentous carbon is not as unambiguous as supposed earlier. Probably, silicate species can both inhibit and promote the process depending on their concentration in the catalyst. It will also be demonstrated below that they can affect the structure and morphology of the filaments.

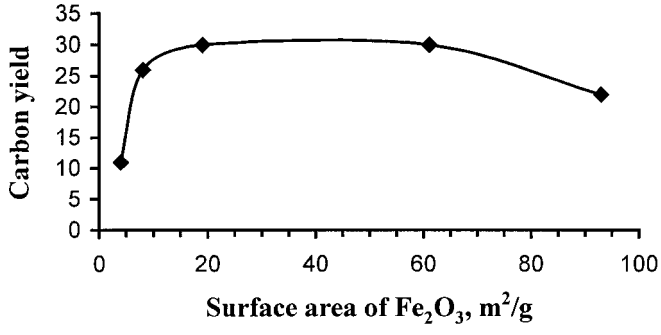

FIG. 4. Yield of carbon (g/g Fe) on silica-stabilized iron catalyst (10%SiO_2–90%Fe) as a function of specific surface area of the initial iron oxide.

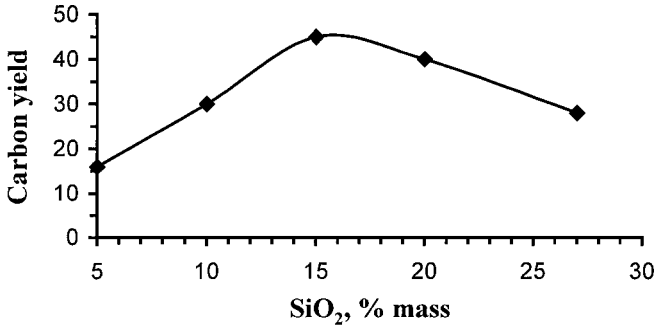

FIG. 5. Yield of carbon (g/g Fe) as a function of content of SiO_2 in iron catalysts (iron oxide was calcined at 500°C before the promoter was introduced).

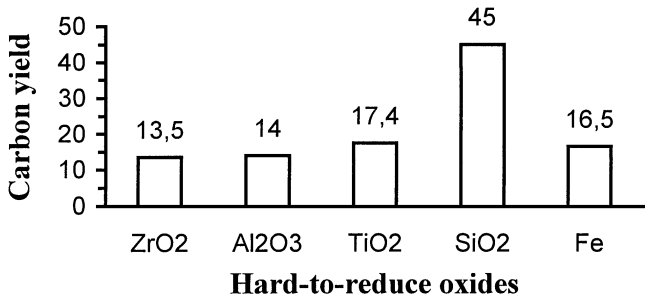

FIG. 7. Influence of the chemical nature of hard-to-reduce oxide on the yield of carbon (g/g Fe) (iron oxide was calcined at 500°C before the promoter was introduced).

Another argument for this assumption is found in Fig. 5, which shows the yield of carbon as a function of the amount of SiO_2 in the catalytic system. It is seen that the maximal yield is obtained with the catalyst containing 15 wt% of silica. An exciting fact is that the catalyst containing 5 wt% of silica provides even lower carbon yield than iron alone. If the silica content increases to above 15 wt%, the yield decreases again, this effect being less pronounced though.

Studies of the behavior of silica-promoted catalysts at different temperatures demonstrated (Fig. 6) the dependence of the carbon yield on temperature, which resembles that obtained with bare iron. The only difference was the quantity of carbon formed. At the range of optimal temperatures, the yield obtained with the promoter catalyst reached 45 g per of iron against 16 g with bare iron. It is interesting that carbon formed with iron catalysts, unlike the carbon synthesized on nickel catalysts, is in the form of loose, weakly bonded conglomerates to be easily powdered. We showed earlier (29) that the decomposition of methane on high-loaded nickel–silica catalysts produced strong and firm carbon granules; the attrition resistance of these granules was higher the longer the reaction time and the higher the carbon yield. Similar dependences could not be established for the carbon formed on iron–silica catalysts.

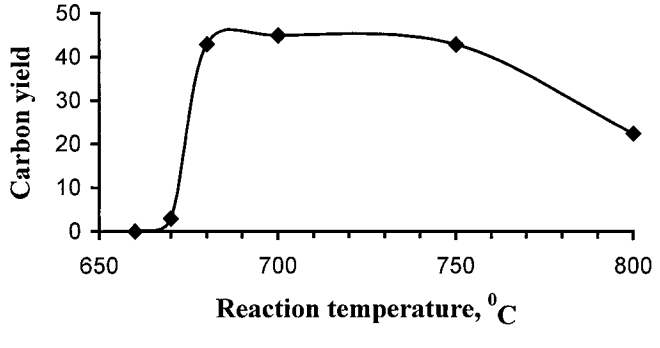

FIG. 6. Yield of carbon (g/g Fe) as a function of reaction temperature. Catalyst: Fe/SiO_2 containing 15 wt% of silica.

The experiments with iron and silica-promoted iron catalysts allowed the optimal temperature regime and the optimal percentage of the catalyst components to be determined. The other iron-based systems were tested under these conditions. Al_2O_3, TiO_2, and ZrO_2 were used as hard-to-reduce oxides. DTG curves for reduction of the oxide systems are plotted in Fig. 3. Al_2O_3- and ZrO_2-containing iron oxides are seen to be almost completely reduced at 600–700°C, whereas the reduction of TiO_2-promoted iron oxide is finished at above 750°C. Thus, the presence of titanium oxide results in the shifting of the temperature of reduction of iron oxide toward higher temperatures compared to the other promoters. In general, iron is more liable to formation of hard-to-reduce intermetallic compounds than, e.g., nickel. Figure 7 demonstrates how the chemical nature of the hard-to-reduce oxide introduced into the catalyst influences the carbon yield in comparison with pure iron. None of the textural promoters except SiO_2 is seen to provide a considerable increase in the carbon yield, some decrease in the yield being observed in the presence of alumina and zirconium oxides. It was mentioned above that silica appeared the best promoter for increasing the carbon yield upon decomposition of methane on nickel catalysts (7). As to the rest of the promoters under study, the worst promoter was TiO_2, while ZrO_2 and Al_2O_3 revealed approximately equal efficiencies and took the place between TiO_2 and silica. For the case of iron, the effect of TiO_2 is opposite, and the carbon yield is higher in the presence of TiO_2 than in the presence of zirconium oxide or alumina.

3.3. Influence of Chemical Nature of Hard-to-Reduce Oxide on the Morphology and Structure of Filamentous Carbon

Apart from the yield of carbon, another important parameter of the process of methane decomposition is potentiality of controlling the morphology and structure of the produced filamentous carbon.

Carbon samples obtained on promoted iron catalysts and on iron alone were studied in the present work using

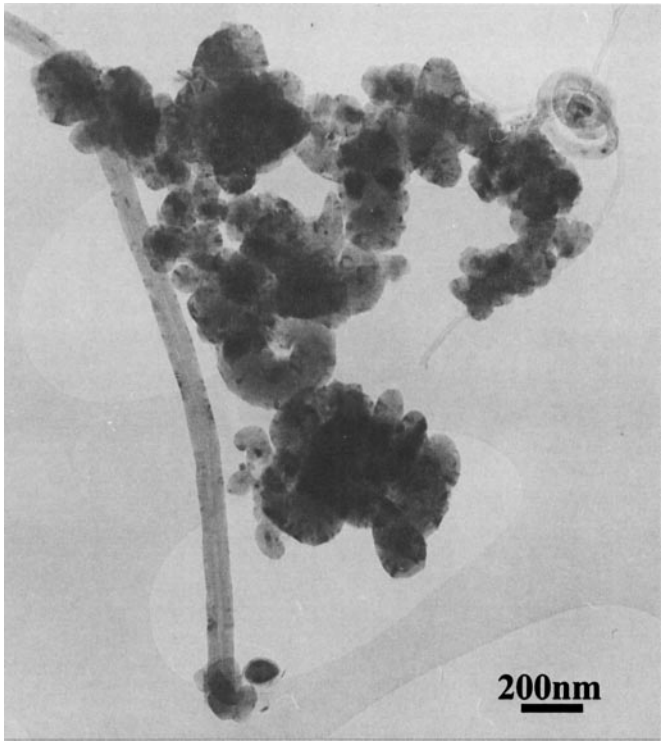

FIG. 8. Carbon synthesized on bare iron (carbon yield is 16 g/g Fe).

high-resolution electron microscopy. The results obtained elucidated that introduction of a hard-to-reduce oxide influences remarkably the carbon morphology. Figure 8 is a micrograph of carbon synthesized on iron alone. A major part of the carbon looks like short, thick filaments rolled up into shapeless tangles and capsules around metal particles. Besides, there are long straight filaments and even thin-walled tubes in negligible amounts. Another case is when iron is promoted with 15% of TiO_2 (Fig. 9). Filaments stop curling into tangles; they are seen to be very bent and often twisted along their axis. The filament shape is random and nonuniform, they became thicker or finer as they grew. Visually, there are mainly large-diameter filaments (100–200 nm) and a scarce proportion of fine filaments. Absolutely different morphology is characteristic of carbon synthesized on Fe/SiO_2 (Fig. 10). There are mainly thick-walled tubes of different diameters shaped as bamboo-like structures. They look like chains in two-dimension micrographs. Inclusions of round-shaped metal particles are often seen inside the tubes (Fig. 11). There are also continuous thick filaments, but not often. Besides, there are thin-walled tubes in a negligible amount. Carbon produced on Fe/ZrO_2 (Fig. 12) and carbon produced of Fe/Al_2O_3 (Fig. 13) resemble one another. Filaments are mainly shaped as hollow tubes. They are longer and bend less than the above-described samples. In particular, chain-like filaments are not characteristic of these carbons. However, there is the same difference between them. For example, it is striking that the walls of tubes synthesized with Fe/Al_2O_3 are finer than those obtained with Fe/ZrO_2. It is also striking that the tips of tubes obtained on Fe/Al_2O_3 are free of metal particles, only empty ends of the tubes are seen in the micrographs.

Thus, the hard-to-reduce oxide under study cannot be considered as exceptionally textural promoters; they

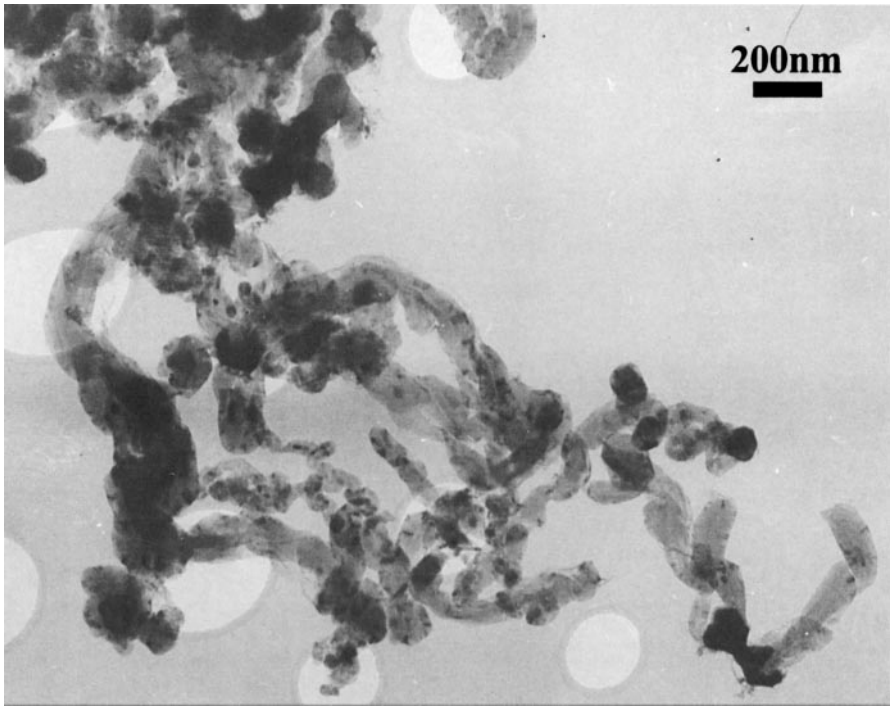

FIG. 9. Carbon synthesized on Fe/TiO_2 catalyst (carbon yield is 17.4 g/g Fe).

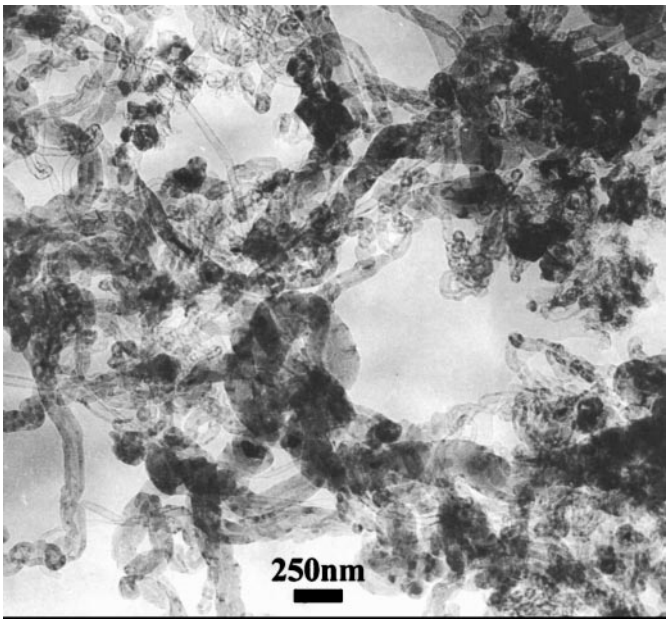

FIG. 10. Carbon synthesized on Fe/SiO_2 catalyst (carbon yield is 45 g/g Fe).

interact with iron to have an evident impact upon the carbon morphology. Structural and textural characteristics of carbon deposits synthesized with iron catalysts are presented in Table 2 as dependent on the nature of the hard-to-reduce oxide.

The data obtained show that the specific surface area of the carbon samples ranges between 20 and 79 m^2/g, and the pore volume ranges between 0.13 and 0.27 cm^3/g. Micropores were not observed in the carbon samples except those obtained with Fe/SiO_2 catalyst (the micropores were 0.011 cm^3/g in volume). Therefore, the latter sample possesses the highest specific surface area among the others. The low specific surface area of the carbon produced on Fe/Al_2O_3 is somewhat surprising because fine nanotubes with thin walls are seen in a huge amount in the micrographs (Fig. 13). Hence, the hollows of these tubes is inaccessible to molecules of the adsorbate gas and, for this reason, cannot be determined using adsorption methods. Apparently, there are fine partitions composed of several graphite layers, which divide the inside space of the tubes and make it inaccessible (Fig. 14).

For graphite-like carbons, the degree of graphitization is often judged by the interlayer distance (d_{002}) determined from the position of diffraction line 002 (30). The graphitization degree of carbon samples is calculated by the Maire and Mering formula

$$\mathbf{d} = 3.354 + 0.086\,(1 - \mathbf{g}),$$

where **d** is interplane distance (d_{002}) in angstroms, **g** is graphitization percentage. If $d_{002} = 3.35$Å, the graphitization degree is taken as a unit; the higher d_{002}, the lower graphitization degree. The limit $d_{002} = 3.44$Å is an empirical value chosen by analysis of the large number of experimental data. Pertinent XRD data show more or less disordered structure characteristic of all the samples synthesized with iron catalysts, the graphitization degree being from 49% for the case of iron alone to 0 for Fe/SiO_2. The interplane distance equal to 0.344 nm determined for this sample is the limit point where carbon can be considered as graphite-like. However, the narrow and sharp shape of the peak (d_{002}) for this sample allows the conclusion on the high contribution of crystallites. Additionally, well-structured extended graphene layers, which are predominantly oriented along the filament axis, are clearly seen in the HREM images (Figs. 11 and 14). It seems reasonable to suggest that the interplane distance increases because carbon atoms or clusters, which preserve their sp^3 hybridization due to bonding with hydrogen, are included in the graphite structure (31). It was elucidated before that a rather high proportion of this kind of carbon is always characteristic of filamentous carbon synthesized from methane. Again, the low graphitization level is traditionally accounted for by the turbostratic structure of filamentous carbon, i.e., by the extreme curvature of the graphene layers. This is particularly true for filament of coaxial cylindrical or coaxial conical structure with a narrow hollow center. If the filaments are not hollow (this is the case of, e.g., carbon synthesized on iron alone or iron–titanium catalysts), the graphitization degree is higher. For the same reason, the graphitization degree is higher for the case of Fe/Al_2O_3 catalyst (thin-walled nanotubes with wide

TABLE 2

Textural and Structural Characteristics of Filament Carbons Synthesized Using Different Iron Catalysts at 700°C

Catalyst	Specific surface area, m^2/g	Pore volume, cm^3/g	Micropore volume, cm^3/g	Average pore diameter, nm	Interplanar distance (d_{002}), nm	Coherent scattering regions (d_{002}), nm	Degree of graphitization (g), %
Fe	48.14	0.15	—	12.5	0.3396	12.8	52
Fe/SiO_2	71.14	0.27	0.011	15	0.344	8.7	0
Fe/Al_2O_3	44.55	0.22	—	19.8	0.341	9.5	35
Fe/ZrO_2	63.59	0.21	—	13.5	0.3417	8.7	27
Fe/TiO_2	21.84	0.12	—	23.35	0.340	11.5	46

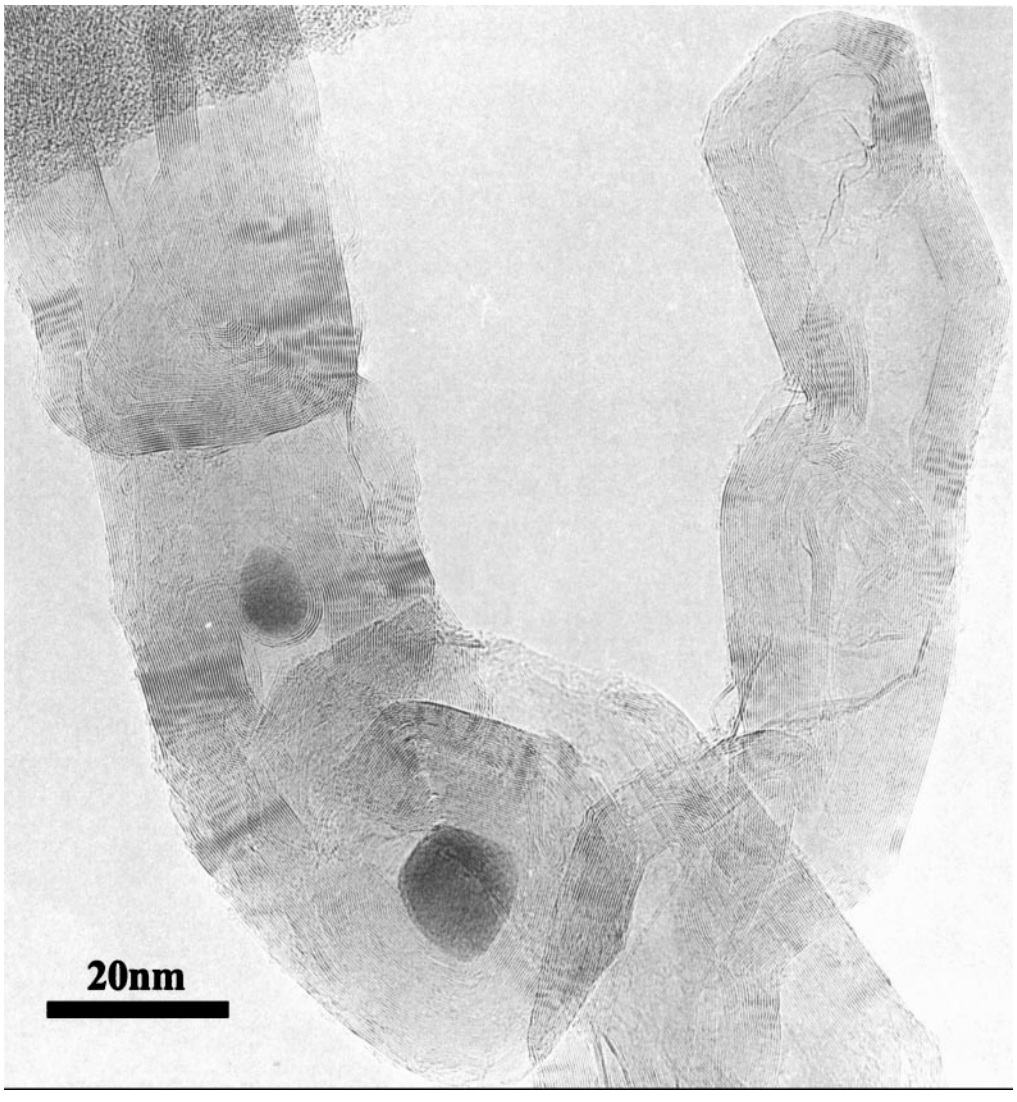

FIG. 11. Metal particles inside carbon filaments (catalyst is 85% Fe-15% Al_2O_3).

inner channels) than for Fe/ZrO_2 (thicker-walled tubes with narrow inner channels). As to the carbon synthesized on the iron–silica catalyst, it is predominanly constituted by thick-walled nanotubes of different diameters, which are additionally twisted around their axis. Probably, this is the factor, which is responsible along with the factor mentioned above, for the higher interplane distance (d_{002}) compared to that of graphite.

3.4. Specific Features of Carbon Filament Formation from Methane on the Iron Catalysts

Some specific features are characteristic of the process of formation of carbon filaments on the iron particles in the methane medium. The iron systems reach their active state in the jump-like manner when the are heated to a certain rather high temperature of 680°C, whereas methane decomposition over the nickel and cobalt catalysts to produce carbon nanofibers starts at 450°C. This phenomenon can be explained in terms of the chemical nature of the iron–carbon interactions Pilipenko and Veselov (32) investigated the formation of cementite at interactions of powdered iron and methane. They showed that at 450–650°C iron was fully transformed into Fe_3C (cementite). Fe_3C alone did not reveal catalytic activity to decomposition of hydrocarbons; therefore uncombined carbon was not detected in the samples. At 700° C, the sample was not 100% cementite but always comprised the phase of α-Fe. The presence of carbon in the sample was detected by XRD after a few minutes of the reaction. Progressive decomposition of cementite into α-Fe and carbon started after this point. Similar results on carbide formation on hematite were also reported by Buyanov and Chesnokov (33). They classified three temperature ranges: the first range was below 500°C at the rate

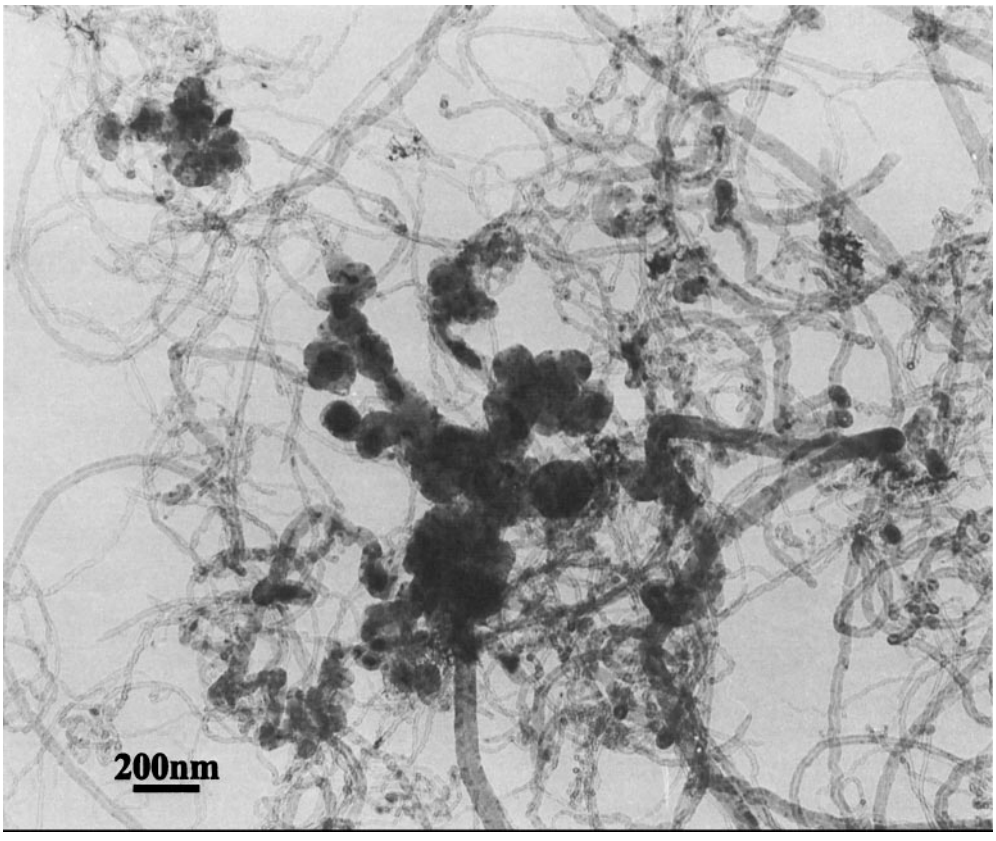

FIG. 12. Carbon synthesized on Fe/ZrO_2 catalyst (carbon yield is 13.5 g/g Fe).

of formation of carbide higher than the rate of its decomposition. At the second range between 500 and 725°C, the rate of formation of carbide was initially higher than the rate of its decomposition but then, as soon as graphite phase nuclei were accumulated, the rate ratio changed and the catalyst was gradually transformed into the metal phase. The third range was above 725°C, where the rate of carbide decomposition was higher than the rate of carbide generation and the iron phase was stable from the outset. Thus, we can suppose that the observed temperature threshold at 680°C corresponds to the point where iron carbide is transformed into its metastable state and the α-iron phase is formed in a considerable amount, the latter being active to decomposition of hydrocarbons.

We shall consider the arrangement of iron–carbon systems with $Fe–Al_2O_3$ as an example. When put into a hydrocarbon medium above 680°C, iron particles start producing oriented growth of carbon structures. The catalyst shown in Figs. 15 and 16 is at the early stage of the reaction after the increase in weight of the sample has reached 150 wt%. The metal is seen to be often pulled into the hole of close-end tubes (Figs. 15a and 15b) in the course of carbon growth. That can be hardly explained unless the quasi-liquid state of the catalytic particles is assumed. Metal-filled carbon nanotubes, also called nanowires, are usually seen when the experiment is conducted at a very high temperature above the metal melting point, for example in a voltaic arc or in an exploded hydrocarbon mixture containing catalytically active metals. Empty carbon capsules are also seen in the micrograph (Fig. 15a). Again, various exotic structures are formed which are built up by accrete graphite capsules, both empty and metal-filled (Fig. 16). Long, thin-walled carbon tubes (Fig. 13) are observed in samples of completely carbonized catalysts but not at the early the stage of their growth. It looks like the tubes grow on fine enough, less than 20 nm in size, growth centers formed through dispersion of the coarse (100–200 nm) particles which predominate during the early hours of the reaction. How can iron particles adopt quasi-liquid properties at temperatures far below the melting point of the iron–carbon eutectic? Krivoruchko *et al*. (34) reported earlier the attainability of liquid state of iron–carbon compounds at anomalously low temperatures. Their *in situ* experiments were conducted in vacuum directly in a chamber of an electron microscope by heating goethite particles (α-FeOOH) supported on amorphous carbon. The particle chemical composition was controlled based on the set of microdiffraction reflections. Quasi-liquid iron-containing particles at 640°C were observed. The particles were continuously reshaped, they moved through the support (the authors

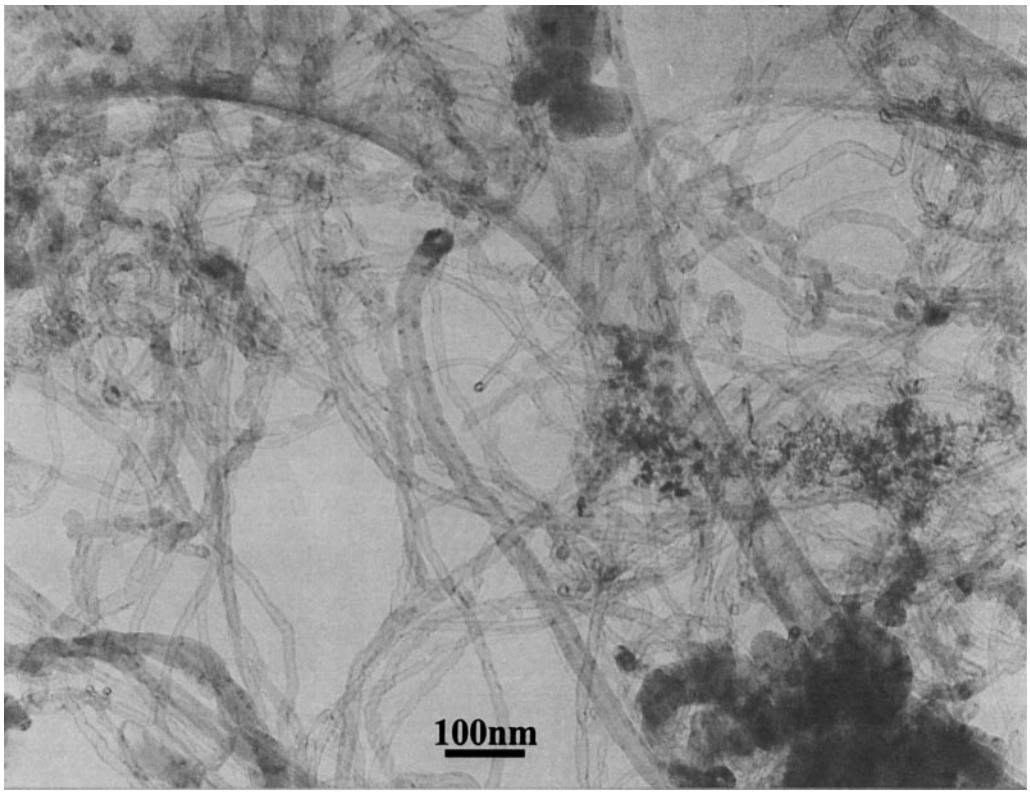

FIG. 13. Carbon synthesized on Fe/Al_2O_3 catalyst (carbon yield is 14 g/g Fe).

used video recording) and left graphite tracks behind them. Apart from visual observations, the disappearance of microdiffraction reflections from particles and of diffraction contrast typical of crystals also argued the quasi-liquid state. An elevation and diminution of temperature resulted in an increase or decrease, respectively, in the rate of particles motion. When the particles stopped as a result of temperature diminution, the set of pertinent microdiffraction reflections allowed the probable formula of the metastable carbide to be established. In their opinion, it was FeC, comprising carbon in amounts of 17.6 wt%. The particles, when cooled abruptly to room temperature, remained in the form of FeC. If they were maintained at 600°C, they transformed into Fe_3C to release excess. Thus, the authors attributed the quasi-liquid state of iron–carbon particles to the formation of an unusual carbide structure. However our XRD studies did not reveal any unusual structures but only α-Fe, cementite, and graphite in the catalysts cooled abruptly after 1 h operation. The content of cementite decreased in fully carbonized Fe/Al_2O_3 catalysts (carbon yield 14 g per g Fe). An interesting phenomenon was that α-Fe and graphite but absolutely no cementite were observed in XRD patterns of Fe/SiO_2 catalysts after deposition of 45 g of carbon on them.

Buyanov (35) suggested another explanation of the unusual fluidity of catalytic particles at anomalously low temperatures. From his viewpoint, the close-packed arrangement of crystal lattices of transition metals which have small atom radii (0.126 nm for Fe and 0.124 nm for Ni), provides an insufficient room for carbon atoms (0.077 nm) in its octahedral voids, and the transfer of carbon atoms through the crystal makes the lattice constituents oscillating. This is equivalent to temperature elevation in the system. As a result, the system may transfer into the quasi-liquid state at temperatures far lower than the melting point inherent in it. These speculations lead to the conclusion that iron particles must be in on overheated state with respect to the surrounding temperature during the growth of carbon filaments. However, one fails to fix such a thermal effect. We can only suggest a converse phenomenon, i.e., the carbon atoms are incorporated into the octahedral voids at the moment of expanding of the distance between metal atoms due to heat oscillations (melting-point of massive iron is 1535°C, Tamman temperature $\sim Tm/2 = 767$°C). Naturally, any additional thermal effects will not take place; in this case. Thus, we can conclude that the unusual fluidity of metal particles in the course of transformation of amorphous carbon into graphite take place; however, the cause of this phenomenon is not understood so far.

Comparison of the behavior of nickel and iron nanoparticles with respect to growth of carbon structures allows the following conclusion to be made: iron, unlike nickel, cannot

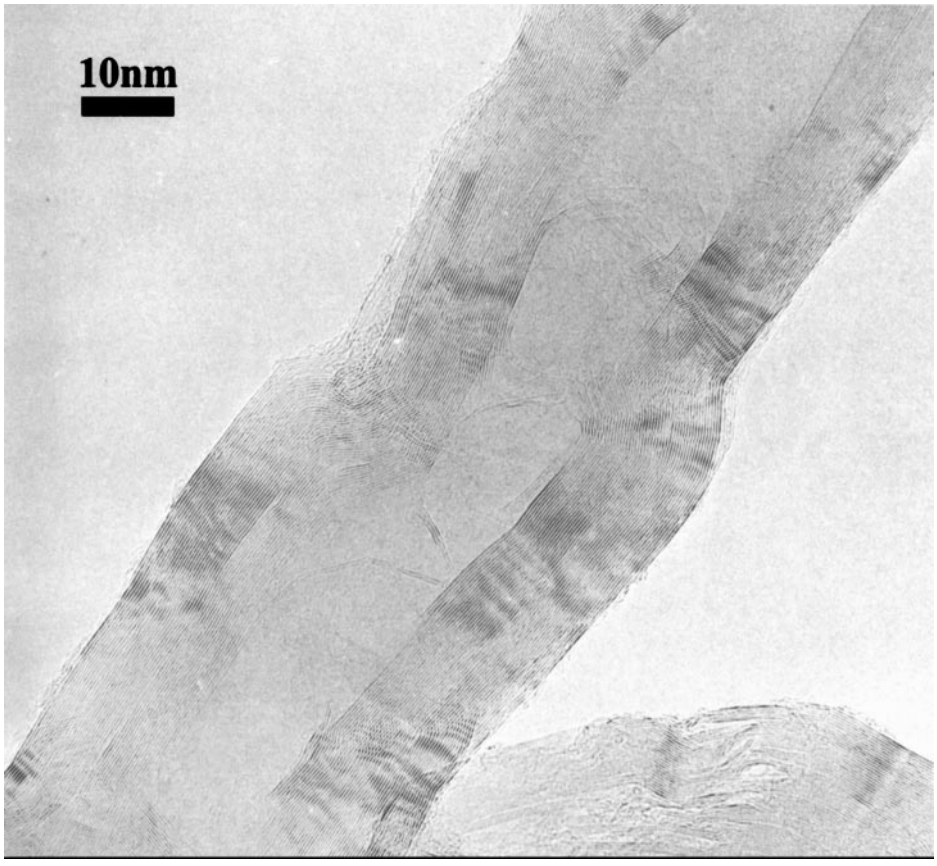

FIG. 14. Fragment of carbon nanotube synthesized on Fe/Al_2O_3 catalyst.

provide decomposition of methane at 400 to 600°C. For the case of nickel, hydrocarbon decomposition and formation of graphite occur on different edges due to anisotropy of nickel crystals. Nickel nanoparticles are always distinctly facetted, and carbon layers are deposited in parallel to the 111 planes at an acute angle to the filament axis. In this case nickel particle is capable of producing carbon in extremely high amounts of 300–400 times its own weight. The iron catalysts operate in a different mode, probably in accordance with the so-called *carbide cycle* suggested by Buyanov (36, 37): carbide Fe_3C which is metastable under certain conditions is decomposed preferably nearby graphite nuclei. Cementite is formed by hydrocarbon decomposition on the free surface fragment of the catalytic particle and disintegrated to form graphitized carbon nearby the graphite-covered surface. The equilibrium is attained as soon as graphite covers some part of the particle surface. The resulting gradient of carbide concentration is the driving force of the carbon diffusion through the iron-carbide particle. Evidently, this model of carbon growth does not need a specific set of edges, as it does for the case of nickel. Moreover, any crystal lattice is not necessary and the particle may be liquid. Figure 17 is a schematic of the stages of nucleation and growth of carbon filaments on an iron-carbide particle. When the catalyst is placed in the methane medium at 680–800°C, iron particles are rapidly carbidized. The carbide is unstable under these conditions. Decomposition of carbide leads to supersaturation of the particle with carbon that results in the emergence of a graphitic nucleus (Fig. 17a.) Since the nucleation must overcome a high activation barrier, other graphite crystals assemble around the former nucleus (Fig. 17b). Then the active interaction between the particle surface and methane starts to result in multiple repetition of the carbide cycle. Notice that graphite layers are initially oriented in parallel to the particle surface. At a certain moment, the particle becomes fluid, its tail is extended, graphite layers are distorted and their orientation changes to form a hollow structure (Figs. 17d–17f). As the nanotube grows further, its part in contact with the particle becomes narrowed and the tail of the particle is very often pulled inside the carbon capsule (Fig. 17g). Bamboo-like structures are formed in this way. The neck of the graphite tube is even more narrowed, and the particle fragment inside the cavity is cut off. The graphite layers become oriented perpendicular to the particle surface by that moment. Since the contact area between the metal and graphite becomes so small as not to provide equilibrium between the carbon dissolution and graphitization rates, "superfluous"

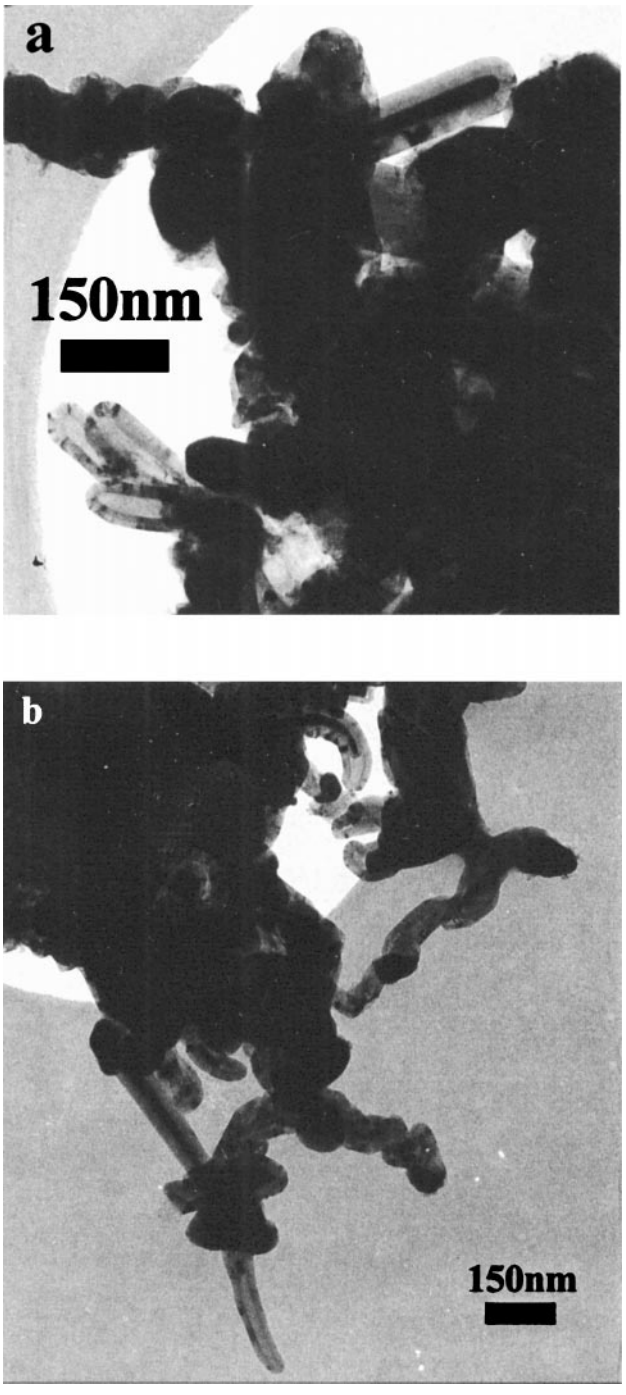

FIG. 15. Carbon synthesized on Fe/Al_2O_3 (carbon yield is 1.5 g/g Fe).

carbon is discharged in the form of additional graphite crystals. They cover a surface fragment adjacent to the already growing tube (Fig. 17h) and initiate construction of the next "bamboo" node.

Apparently, the low yield of filamentous carbon observed with iron catalysts can be accounted for, based on the above scheme, by fragmentary dispersing of fluid iron-carbide particles accompanied by pulling their tails inside the growing graphite tubes. In other words, considerable fragments of particles appear encapsulated by carbon during the filament growth and absolutely isolated from the reaction medium.

If simultaneous crystallization of several graphite nuclei on different surface fragments of an iron carbide particle becomes for any reason possible, the growth of several carbon nanotubes at once is not contradictory to the scheme under discussion and, therefore, cannot be excluded. We revealed structures of this kind when we studied carbon produced on Fe/Al_2O_3. An iron particle, which can be the growth center of several nanotubes, is shown in Fig. 18. The following observations underlay our assumption that this particle is the center of growth and not merely overlies the nanotube agglomerate. The particle in the micrograph is not encapsulated by carbon because the carbon layer necessary for the particle isolation from the reaction medium must be much thicker. All the encapsulated particles detected in micrographs were covered by the carbon layer not thinner than 10 nm. As to the micrograph under consideration, the graphite shell around the particle is not thicker than 3 nm, i.e., its possible origin is carbon released during the carbide decomposition at the sample cooling. If the particle is not encapsulated, it can produce filamentous carbon in the hydrocarbon medium at high temperatures. We believe that this particle is responsible for the formation of at least a part of the nanotubes adjacent to it. Besides, another argument for this assumption is that the particle is in the very center of the nanotube agglomerate. The radial growth mode of one-wall carbon nanotubes on a round nickel carbide particle was demonstrated earlier by Saito (38). Saito

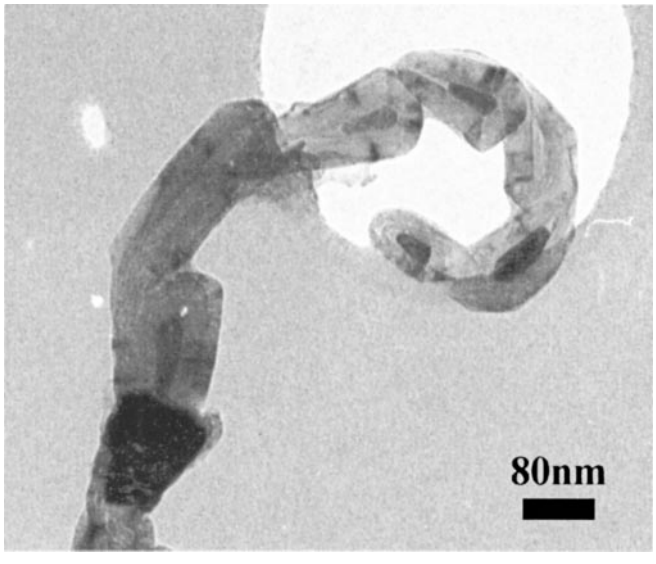

FIG. 16. Bamboo-like filament (Fe/Al_2O_3, carbon yield is 1.5 g/g Fe).

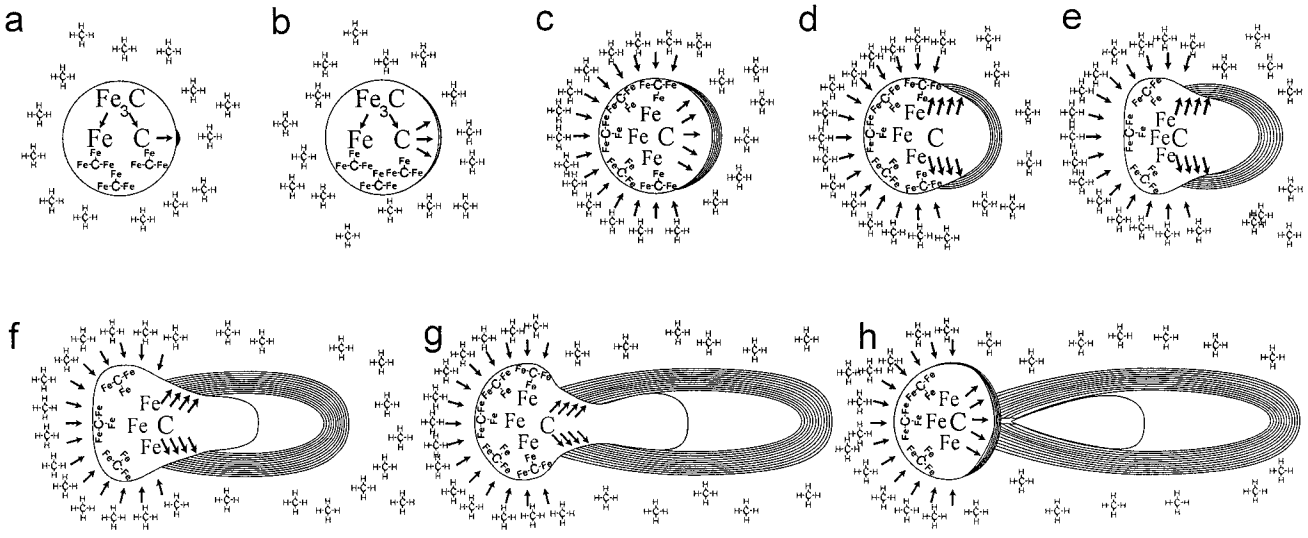

FIG. 17. Scheme of stages of nucleation and growth of carbon filaments on an iron-carbide particle.

observed these structures in carbon deposits produced by co-evaporation of a metal and carbon in voltaic arc, i.e., at the conditions not allowing the solid state of the metal phase.

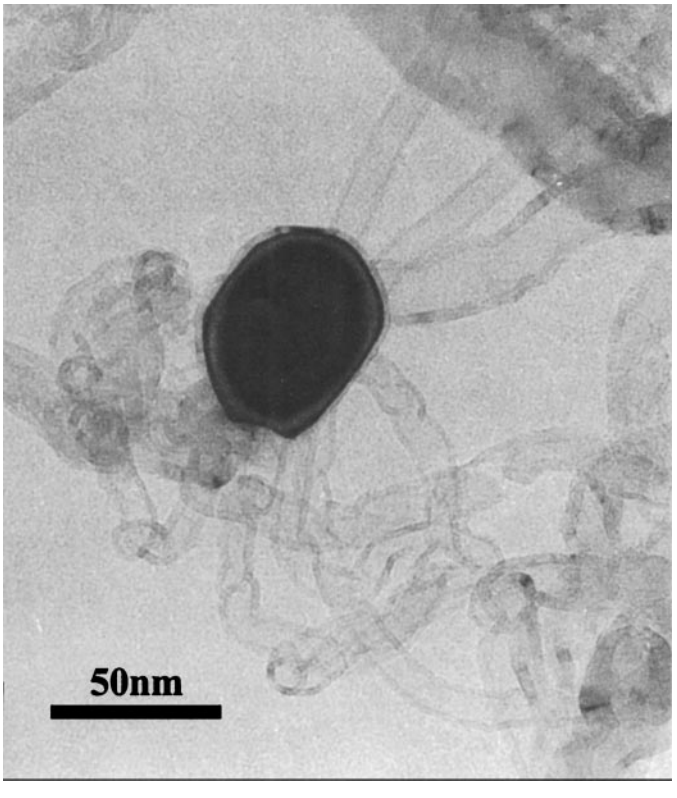

FIG. 18. Octopus-like centers of nanotubes growth in carbon deposits formed on Fe/Al_2O_3 catalyst (carbon yield is 14 g/g Fe).

4. CONCLUSIONS

The temperature threshold, above which the process of methane decomposition on α-Fe became stable and could be maintained for a long period of time, was exactly determined. The reaction was sharply accelerated after the temperature had reached 680°C, the yield of carbon being many times increased to reach the maximum at the level of 16–17 g per g of iron. Apparently, this temperature corresponds to the point of transition of iron carbide from a stable to metastable state. Simultaneous presence of both α-iron and carbide phases in the catalytic particle is thought to be necessary for oriented growth of carbon on it.

When iron oxide was not promoted by hard-to-reduce oxides, only the reduction temperature but not texture influenced the rate of growth of carbon filaments.

In the case of high temperature (higher than 800°C) reduction, the process of filament growth was slowed down even though further reaction was conducted at the optimal temperature range. Hence, coarse iron particles cannot be dispersed in the methane medium. Vice versa, the presence of nanoparticles of optimal size in the reduced catalyst has a favorable effect upon the carbon yield.

It was established that decomposition of methane on iron catalysts was fully inhibited by alkali metal compounds, even when their proportion was not higher than 1 wt% in the catalyst.

The influence of some hard-to-reduce oxides on the ability of iron to decompose methane was studied. The most promising results on extending the catalyst lifetime were obtained with silica used as an additive to iron. The catalyst comprising silica in the amount of 15 wt% provided carbon yield as high as 45 g per gram of iron. A considerable influence on the carbon yield in comparison to that obtained

with bare iron catalysts was not observed upon the introduction of the other hard-to-reduce oxides, such as TiO_2, ZrO_2, and Al_2O_3.

TEM studies of the carbon deposits demonstrated that the morphology of carbon filaments, unlike the carbon yield, was strongly dependent on the chemical nature of the hard-to-reduce oxides introduced into the iron catalyst. With bare iron, the carbon was mainly produced as shapeless tangles of short helical filaments, whereas introduction of textural promoters resulted in synthesis of lower bended long filaments, continuous or hollow, each oxide being responsible for synthesis of carbon of unique morphology.

Metal-filled carbon nanotubes were observed in carbon deposits at 1 h from the reaction onset. This is indirect evidence of high fluidity of iron–carbon particles during transformation of amorphous carbon to graphite at unusually low temperature that had been assumed by other researchers. We also believe that the preferable mechanism of the catalyst deactivation in the temperature range under study is the fragmentary dispersion of iron nanoparticles. The dispersion is accompanied by simultaneous encapsulation of broken particle fragments by growing carbon.

REFERENCES

1. Hughes, T. V., and Chambers, C. R., U.S. Patent 405480 (1889).
2. Figueiredo, J. L., Bernardo, C. A., and Baker, R. T. K. (Eds.), "Carbon Fibers Filaments and Composites." Kluwer Academic, Dordrecht/Norwell, MA, 1990.
3. Chesnokov, V. V., Zaikovskii, V. I., Buyanov, R. A., Molchanov, V. V., and Plyasova, L. M., *Kinet. Katal.* **35**, 146 (1994).
4. Avdeeva, L. B., Goncharova, O. V., Kochubey, D. I., Novgorodov, B. N., Plyasova, L. M., and Shaikhutdinov, Sh. K., *Appl. Catal. A* **141**, 117 (1996).
5. Li, Y., Chen, J., and Chang, L., *Appl. Catal. A* **163**, 45 (1997).
6. Zhang, T., and Amiridis M. D., *Appl. Catal. A* **167**, 161 (1998).
7. Ermakova, M. A., Ermakov, D. Yu., Kuvshinov, G. G., and Plyasova, L. M., *J. Catal.* **187**, 77 (1999).
8. Ermakova, M. A., Ermakov, D. Yu., and Kuvshinov, G. G., *Appl. Catal. A* **201**, 61 (2000).
9. Otsuka, K., Kobayashi, S., and Takenaka, S., *Appl. Catal. A* **190**, 261 (2000).
10. Gadelle, P., *in* "Carbon Fibers Filaments and Composites" (J. L. Figueiredo, C. A. Bernardo, and R. T. K. Baker, Eds.), p. 95. Kluwer Academic, Dordrecht/Norwell, MA, 1990.
11. Benissad, F., Gadelle, P., Coulon, M., and Bonnetain, L., *Carbon* **26**, 61 (1988).
12. Tibbets, G. G., Devour, M. G., and Rodda, E. J., *Carbon* **25**, 367 (1987).
13. Tibbets, G. G., and Balogh, M. P., *Carbon* **37**, 241 (1999).
14. Walker, P. L., Rakszawsri, J. F., and Imperial, G. R., *J. Phys. Chem.* **63**, 133 (1959).
15. Kawasumi, S., Egashira, M., and Katsuki, H., *J. Catal.* **68**, 237 (1981).
16. Baker, R. T. K., Alonzo, J. R., Dumesic, J. A., and Yates, D. J. C., *J. Catal.* **77**, 74 (1982).
17. Robertson, S. D., *Carbon* **8**, 365 (1970).
18. Evans, E. L., Thomas, J. M., Thrower, P. A., and Walker, P. L., *Carbon* **11**, 441 (1973).
19. Baker, R. T. K., and Thomas, R. B., *J. Cryst. Growth* **12**, 185 (1972).
20. Galuszka, J., and Back, M. H., *Carbon* **22**, 141 (1984).
21. Sacco, A., Thacker, P., Chang, T. N., and Chiang, A. T. S., *J. Catal.* **85**, 224 (1984).
22. Avdeeva, L. B., and Shaikhutdinov, Sh. K., *in* "EuropaCat-IV," p. 559, Italy, Rimini, 1999.
23. Hernadi, K., Fonseca, A., Nagy, J. B., Siska, A., and Kiricsi, *J., Appl. Catal. A* **199**, 245 (2000).
24. Kuvshinov, G. G., Ermakova, M. A., and Ermakov, D. Yu., Patent Russia 2126718, Boreskov Institute of Catalysis, 1999.
25. Buyanov, R. A., Krivoruchko, O. P., and Rizhak, I. A., *Kinet. Katal.* **13**, 470 (1972).
26. Darken, L. S., *Trans. AIME* **180**, 430 (1949).
27. Baker, R. T. K., Chludzinski, J. J., and Lund, C. R. F., *Carbon* **25**, 295 (1987).
28. Kepinski, L., *Carbon* **30**, 949 (1992).
29. Kuvshinov, G. G., Mogilnykh, Yu. I., Kuvshinov, D. G., Ermakov, D. Yu., Ermakova, M. A., Salanov, A. N., and Rudina, N. A., *Carbon* **37**, 1239 (1999).
30. Maire, J., and Mering, J., *in* "Proc. 4th Biennial American Carbon Conference," p. 345, 1960.
31. Ruland, W., *Carbon* **2**, 365 (1965).
32. Pilipenko, P. S., Veselov, V. V., *Poroshk. Metall.* **150**(6), 9 (1975).
33. Chesnokov, V. V., and Buyanov, R. A., *Kinet. Katal.* **28**, 403 (1987).
34. Krivoruchko, O. P., and Zaikovskii, V. I., *Kinet. Katal.* **39**, 607 (1998).
35. Buyanov, R. A., and Chesnokov, V. V., *Khim. Interesakh Ustoich. Razvit.* **3**, 177 (1995).
36. Buyanov, R. A., Chesnokov, V. V., Afanas'ev, A. D., and Babenko, V. S., *Kinet. Katal.* **18**, 839 (1977).
37. Chesnokov, V. V., and Buyanov, R. A., *Russ. Chem. Rev.* **69**, 623 (2000).
38. Saito, Y., *Carbon* **33**, 979 (1995).